Investigation of an elementary model for magnetic froth

1991 J. Phys.: Condens. Matter 3 2101

(http://iopscience.iop.org/0953-8984/3/13/013)

J. Phys.: Condens. Matter 3 (1991) 2101–2114. Printed in the UK

Investigation of an elementary model for magnetic froth

D Weaire†, F Bolton†, P Molho‡ and J A Glazier§

† Department of Physics, Trinity College, Dublin 2, Ireland

‡ Laboratoire Louis Néel, 38042 Grenoble Cedex, France

§ AT&T Bell Laboratories, Murray Hill, NJ 07974, USA

Received 28 December 1990

Abstract. The analogy between magnetic froth (cellular domain patterns in garnet films) and the two-dimensional soap froth is used to develop an elementary model for the former system. Simulations are performed using this model: they have many features in common with recent experimental results and can be further illuminated by simple calculations in the spirit of mean-field theory. An analysis of topological cell statistics is also presented.

1. Introduction

Among the various patterns exhibited by the magnetic domain structure of garnet films, cellular domains present a particularly fascinating example of the interplay between energetics, kinetics and geometrical/topological constraints. They have been observed for some time (e.g. Wolfe and North 1974), but have only recently been the object of detailed observation and statistical analysis (Babcock and Westervelt 1989a, b, 1990, Babcock *et al* 1990). Broadly similar observations were made by Molho and described by Glazier (1989); some of these, together with new results for cell areas, are presented here. Experimental details are recorded in Appendix A.

Cellular domains can be created as an ordered hexagonal array or, more interestingly, as a disordered structure in which the cells have different areas and numbers of sides. Examples are shown in figure 1. As this figure illustrates, the structure *coarsens* when the applied magnetic field is gradually increased. This coarsening process proceeds by the progressive elimination of small cells.

The striking similarity of these patterns to those of the two-dimensional soap froth was recognized at an early stage: figure 2 shows such a structure for comparison. This has led us to use the name 'magnetic froth' for the system of magnetic domains (Weaire 1989). Not only are the two structures similar, but there is an obvious analogy between the coarsening of the magnetic froth, as a function of magnetic field, and that of the soap froth, as a function of time. The underlying mechanism is, of course, rather different, but in both cases we are effectively dealing with an evolving equilibrium structure. In the magnetic froth, increasing the magnetic field causes the pattern to coarsen, favouring the direction of magnetization represented as *white* in figure 1. In the soap froth, there is slow diffusion of gas between cells, so the cell areas can be regarded as fixed by a slowly varying constraint.

0953-8984/91/132101 + 14 $03.50

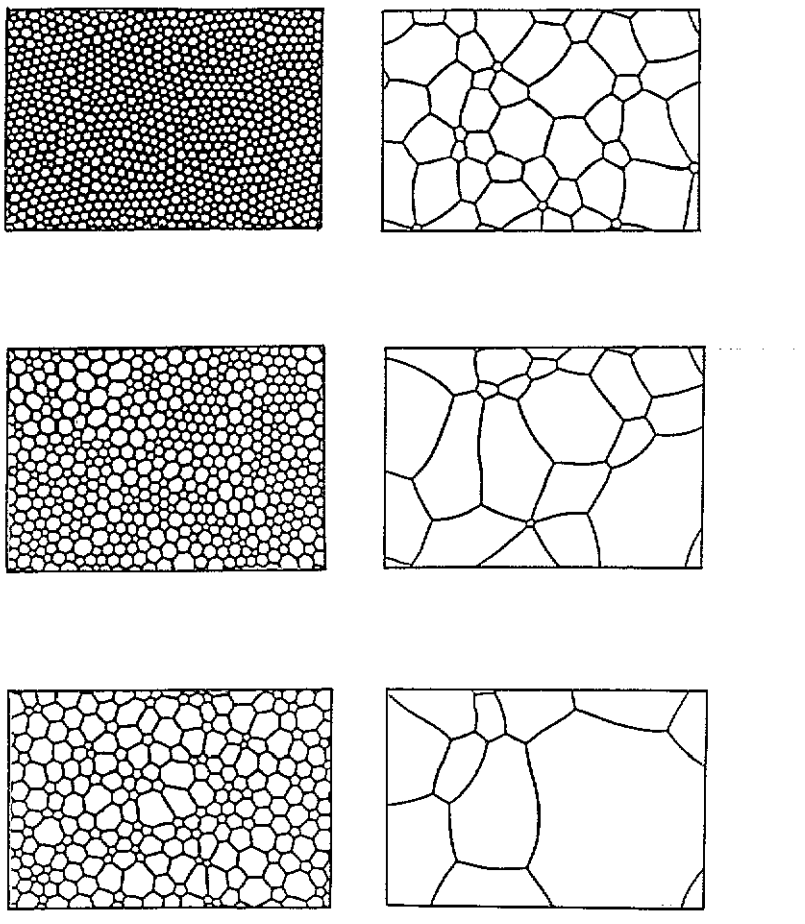

Figure 1. Typical magnetic froth: for experimental details, see Appendix A. The structure is seen to coarsen as the magnetic field H is increased through the following sequence of values: 0, 54.1, 70.5, 85.2, 91.5, 94.8 Oe.

This analogy invites closer attention. The soap froth is now very well understood (see, e.g., Glazier *et al* 1987, Weaire and Lei 1990), and a proven methodology exists for the simulation of equilibrium structure and its coarsening (Kermode and Weaire 1990, Glazier *et al* 1990). This provides an obvious starting point for an attempt to frame an elementary model for magnetic froth. We adopt such a strategy here, defining such a model and identifying some of its properties, by simulation and by various calculations in the spirit of mean-field theory. Before doing so we shall present some relevant experimental data, supplementing the extensive results and of Babcock and co-workers mentioned above.

2. Magnetic froth

As figure 1 shows, the cell walls in magnetic froth are thick, relative to mean cell size, for low magnetic field H (in this case $H \leqslant 30$ Oe), so there are nearly circular magnetic

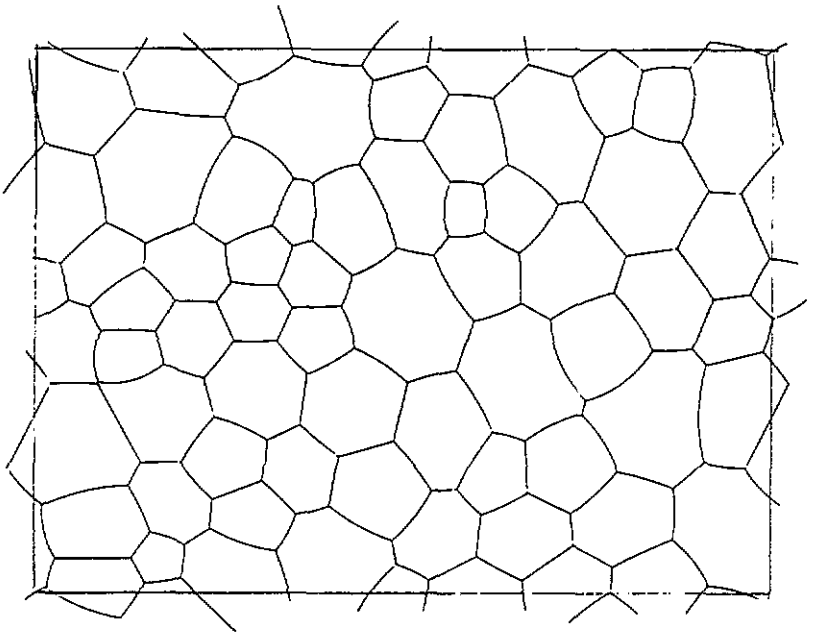

Figure 2. Two-dimensional soap froth, as simulated by Kermode and Weaire (1990).

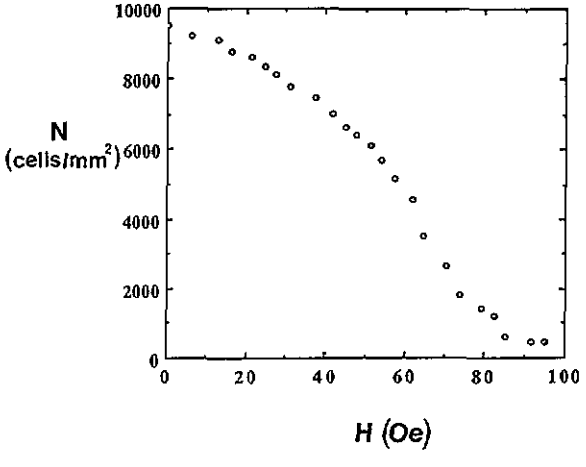

Figure 3. Cell density in magnetic froth as a function of applied magnetic field H, excluding cells at the edge of the sample.

bubbles. Soap froths of relatively high liquid fraction have just this character (Weaire and Bolton 1990), but we shall not pursue the analogy in this limit. For higher magnetic fields, the cell walls are thin and there are clearly defined polygonal cells. Babcock and co-workers made a further distinction, between the intermediate regime and that close to the maximum value of H, at which cell density goes to zero, as shown in figure 3. The latter was called the 'high-tension' regime. In the intermediate regime, n-sided cells with $n < 5$ (of which there are very few, in comparison with soap froths) are eliminated during the early stages of coarsening. Thereafter it is five-sided cells that are eliminated. One

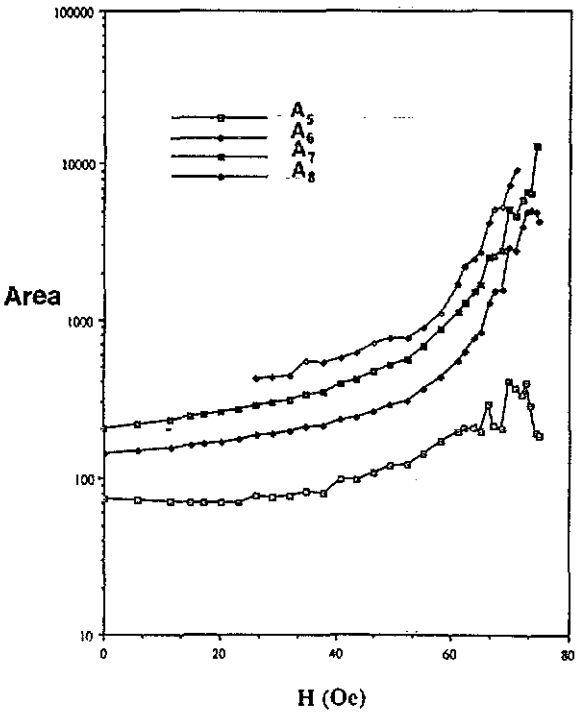

Figure 4. Mean area A_n of n-sided cells (in pixels), as a function of applied magnetic field H.

of the distinguishing features of the high-tension regime is the onset of avalanches of cell eliminations, for which Babcock and Westervelt (1990) have presented extensive statistics.

The intermediate regime is characterized in the data of Babcock and Westervelt (1989b) by a distribution $f(n)$ of numbers of sides of cells that is remarkably constant, so the topological structure remains approximately invariant while the mean area increases by almost two orders of magnitude. The data of Molho for $f(n)$ are slightly different, and will be discussed in a subsequent section. Figure 4 shows the variation of mean area of cells of different types, which has not previously been measured.

We shall now adapt the essentially exact model for soap froth to develop an approximate model for the magnetic froth, in which there are long-range interactions.

3. Model for magnetic froth

We shall first review the essential features of the idealized model of the two-dimensional soap froth. Considering first the case in which liquid cell walls enclose a compressible gas, this is described by the Hamiltonian, for constant total area:

$$E = 2\sigma \sum_i l_i + B \sum_j (A_j - A_{j0})^2. \tag{1}$$

The first sum is over all cell sides i, giving the total cell wall length, to be multiplied by a surface energy (tension) parameter 2σ. The second term arises from the compression/expansion of the gas in which cell: usually the limit of infinite B (i.e. incompressible gas) is taken so that the second term is removed and replaced by the constraint $A_j = A_{j0}$,

where A_{j0} is the area of cell j for gas of constant density. The problem of equilibrating such model structures for the soap froth, such as that of figure 2, then boils down to the assignment of vertex coordinates and cell pressures, such that:

(i) the cell walls have curvatures that balance pressure differences

$$\Delta p_{jj'} = 2\sigma/r_{jj'} \tag{2}$$

where $r_{jj'}$ is the radius of curvature of the cell side between adjoining cells j and j'. It might be noted here that, despite the general visual similarity of soap froths and magnetic froths, a close examination of the latter will reveal cell edges whose curvature is not constant. Clearly, our model will fail to capture this feature.

(ii) the curved cell walls meet at 120° at each vertex (equilibrium of surface tension).

(iii) the appropriate area constraints $A_j = A_{j0}$ are satisfied.

Most of this description and the associated methodology may be generalized to any Hamiltonian of the form

$$E = \lambda \sum_i l_i + F(A_j, A_k, \ldots) \tag{3}$$

consisting of a 'line energy' term together with any function of cell areas *only*.

The equilibrium conditions are (a)

$$\Delta p_{jj'} = \lambda/r_{jj'} \tag{4}$$

where now $\Delta p_{jj'} = p_j - p_{j'}$ and

$$p_j = -\partial F/\partial A_j \tag{5}$$

and (b) vertex angles are 120°, as before.

What form, consistent with (3), is most appropriate for the magnetic froth? Domain wall energy contributes straightforwardly to the line energy term. The applied or bias field H contributes a term proportional to linelength multiplied by the wall thickness, w, which we shall treat as constant throughout the system. Hence increase of H is to be identified with increase of λ, although the zeros of the two quantities are not the same. Not only will we make this assumption but we shall also assume that the wall thickness w does not change with H. This appears to be a reasonable approximation only in the intermediate regime, as discussed below. In any case, a simple correction can be made for the variation of w with H. Finally we are left with the depolarization energy—the dipolar interaction energy of the system—which we shall force into the form of a line energy term, as above, and a simple function of cell areas. This is a somewhat hypothetical approximation, as explained in Appendix B. We argue that the depolarization contribution to the second term may be written as

$$F = \sum_j F_1(A_j) + \sum_{jj'} F_2(A_j, A_{j'}) \ldots \tag{6}$$

where the first sum is over all cells j, the second over nearest-neighbour pairs jj' and so on. It may not be reasonable or practical to extend this series beyond the terms indicated. We shall first consider a model that retains only the single-cell term, and that will prove to be inadequate in certain respects. It will transpire that the addition of the two-cell terms improves matters considerably.

As explained in Appendix B, the proposed forms for F_1 and F_2 are

$$F_1(A_j) = (A_j + C)^{-1/2} \tag{7}$$

(absorbing any constant into the definition of λ), and

$$F_2(A_j, A_{j'}) = \kappa_2(A_j + C)^{1/2}(A_{j'} + C)^{1/2}/[(A_j + C)^{1/2} + (A_{j'} + C)^{1/2}]^3. \tag{8}$$

Here κ_2 is of order unity, and C is a short-range cut-off parameter (deriving from the finite wall thickness). Without such a cut-off, cells would not be forced to disappear as λ is increased. In what follows, the properties of this model are explored without any attempt being made at this stage to match numerical values to those of experiment, which will be a difficult exercise.

4. First-order model

We shall first examine the model defined by equations (3), (6) and (7). While we shall ultimately be forced to revise this primitive model, some of the insights gained are quite general.

We begin by addressing the question posed by figure 4 within the present model: how do mean cell areas vary with increasing λ? We do so by applying a mean-field approximation, surrounding an n-sided cell by n neighbouring cells each of which has area equal to the average over all cells, A_{mean}. We shall also assume equality of pressure in the surrounding cells, so that the central cell under consideration is *symmetric*. By considering the geometry of such a symmetrical cell we can relate the radius of curvature $r_{jj'}$ to the area of the cell, A. The pressure difference is obtained via the derivative of the first-order energy term (equations (5) and (7)) of the cell and its mean-field neighbours. The equilibrium condition (4) now takes the form (in the case $C = 0$, for convenience):

$$2c_n\lambda A^{-1/2} = A_{\text{mean}}^{-3/2} - A^{-3/2}. \tag{9}$$

The constants c_n may be calculated straightforwardly from the area and pressure difference associated with a symmetric n-sided cell, and are negative/positive for $n \lessgtr 6$, and zero for $n = 6$. Note that this implies that the predicted value for a six-sided cell, A_6, equals A_{mean}, within this approximation. An elementary but cumbersome expression for c_n is easily derived: it is well approximated by $c_n = 0.28(n - 6)$.

For low values of λ, there is always a solution A_n (in fact more than one for $n < 6$: the stable solution is the one with higher A). However, this is not the case, whenever a finite cut-off parameter C is included. As λ is increased, the solutions for three, four and five-sided cells cease to exist at critical values of λ: in each case there is a minimum value of A_n (see figure 5).

In a typical disordered network, three- and four-sided cells are not essential and they can be eliminated entirely, with minimal readjustments. However, when we consider the elimination of five-sided cells, the (Euler) requirement, that the mean value of n is exactly six, dictates otherwise. The elimination of individual five-sided cells cannot be expected to reduce the population of such cells to zero unless the system orders itself in the hexagonal structure, which is unlikely. Hence we expect an approach to a steady state in which $f(n)$ remains invariant.

For any given initial value of A_{mean}, consider its subsequent variation with λ. We encounter (after a slight increase of A_{mean}, due to elimination of three- and four-sided cells) a critical value of λ at which five-sided cells are typically unstable, due to loss of the solution of (9). Removal of some such cells increases A_{mean} and this change in cell

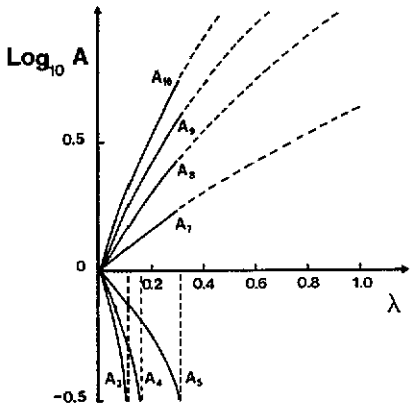

Figure 5. Logarithm of cell area A_n as obtained by solving (9) for A, setting A_{mean} (= A_6) = 1.0 and the cut-off parameter C = 1.0. Three-, four- and five-sided cells become unstable at the points indicated, for this value of A_{mean}.

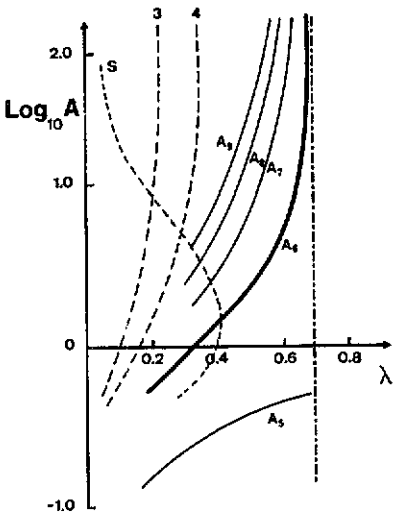

Figure 6. Beyond the point of instability of fivefold cells in figure 5, A_{mean} (= A_6) should vary as shown here (condition of marginal stability). The resulting variations of A_5, A_7, A_8, A_9 are also shown. The trajectories labelled 3 and 4 give the loci of unstability of three- and four-sided cells (cf figure 5). That labelled S denotes the estimated point of the 'spinodal instability', discussed in the text, as a function of A_{mean} and λ.

density is eventually sufficient to stabilize the remainder, for any given increment of λ. According to this argument, A_{mean} is determined by the condition that the typical fivefold cell remains on the margin of stability. This condition of marginal stability can be used to specify A_{mean} for each value of λ. It follows that the curves of figure 5 are irrelevant beyond the point at which the typical five-sided cell is unstable, and we should expect to follow those of figure 6, dictated by marginal stability. Note, in particular, the increase of A_{mean} (coarsening) and its eventual divergence. This occurs at the point at which five-sided cells are typically unstable even at zero density.

It is tempting to try to relate the analytic behaviour of A_{mean} to the scaling analysis performed by Babcock *et al* (1990), but there are a number of complications in doing so. In particular, it is our impression that the result of the above authors ($n \sim (H - H_c)^{2.9}$) relates neither to the intermediate regime (in which we know that the structure is invariant) or to the true asymptotic regime (in which data are sparse) but fits the crossover between them, and may not have fundamental significance.

The variation of the areas of n-sided cells with λ (shown in figure 6) seem broadly consistent with the qualitative form of the data of figure 4. Note that the area differences $A_n - A_{mean}$ are approximately proportional to c_n, for $n > 6$, at least initially.

Having explored the implications of our model in this approximate way, we now turn to direct simulations based upon it. A simulation based on the first-order model was carried out for a disordered structure with initial mean cell area A_{mean} = 6.8 and C = 0.4. Initially, this showed the expected features, including elimination of three- and four-sided cells, as λ was increased (figure 7). Elimination of triples and pairs of five-sided cells should then proceed at critical values of λ. The expected limiting value at

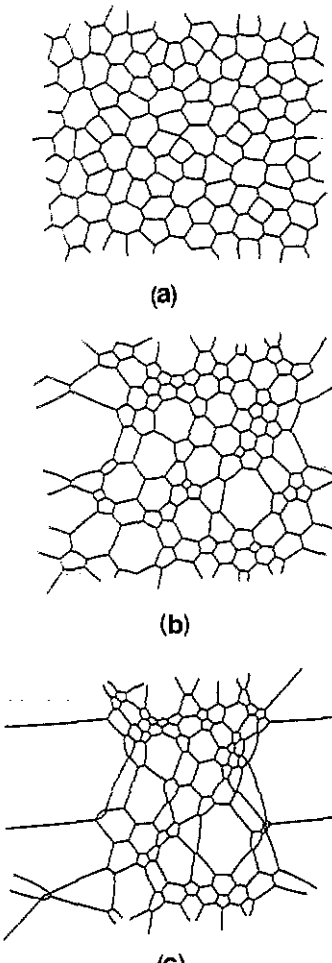

Figure 7. Simulation test of the first-order model, with initial $A_{mean} = 6.75$, $C = 0.4$, showing an instability (separation into regions of large and small cells) at $\lambda \approx 1.2$. Results are shown for $\lambda = 0.06, 0.36, 1.23$.

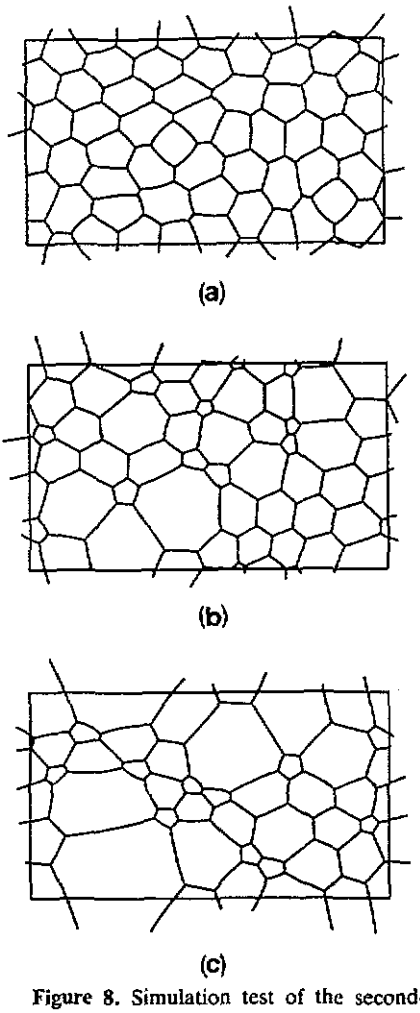

Figure 8. Simulation test of the second-order model, with $\kappa_2 = 1$, $A_{mean} = 2.6$, and $C = 1.0$. Results are shown for $\lambda = 0.01, 0.49, 0.50$.

which cell density vanishes is expected to be $\lambda = 1.7$, based on the earlier arguments of this section, for $C = 0.4$. However, at about $\lambda \approx 1.2$, the structure was found to develop a global instability (figure 7(*c*)) which has no counterpart in experiment for which data are presented here. Something similar does occur when the sample is held at high temperatures, close to the Néel point (see figure 65 of Glazier 1989).

We have been able to understand this behaviour within our model as an analogue of spinodal decomposition: the system becomes unstable with respect to separation into regions of large and small cells. The estimated locus of this instability is shown in figure 6, suggesting that it cannot be avoided by change of parameters. It may be controlled by changing the form of F_1, since the instability is related to the second derivative of this function. However, it seems more reasonable to proceed to the second-order model,

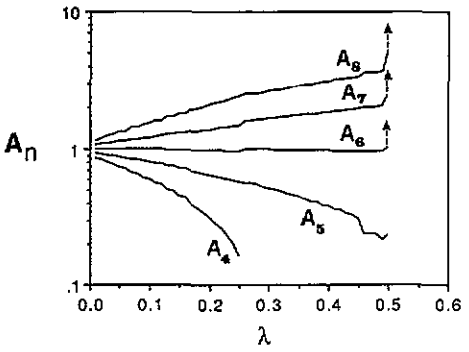

Figure 9. Variation of A_n with λ in the second-order model simulation. All areas are divided by the initial ($\lambda = 0$) mean cell area.

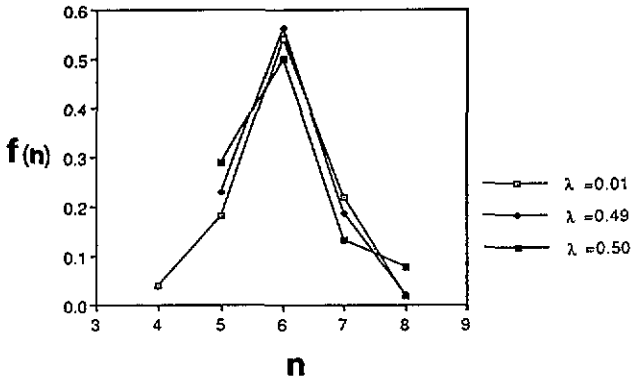

Figure 10. The distribution $f(n)$ of numbers of cell sides for various values of λ, in the second-order model simulation.

which tends to suppress the instability. In any case, it is evident from the analysis of appendix A that the second-order corrections are large.

5. Second-order model

We have assigned the value $\kappa_2 = 1$ in the second-order term defined by (8). This is somewhat arbitrary (see Appendix B) but should be of the right order. Back-of-envelope estimates suggested that the system thus defined should not be subject to the spinodal instability prior to the instability of all five-sided cells. This hope was fulfilled: figure 8 presents some structures obtained with this model. Note first that within a mean-field theory, the *qualitative* expectations are quite similar to those of the first-order model, so we have not repeated that analysis.

We succeeded in following the evolution of this structure over the full range of λ. In one sense, the results are disappointing, in relation to experiment: the system changes from the behaviour that we illustrated by figure 5 to that of figure 6, as expected, but its coarsening behaviour is already dominated by avalanches, so no smooth coarsening is observed. The corresponding area variations are shown in figure 9. The relative areas of n-sided cells, as observed in experiment (figure 4), are quite well reproduced.

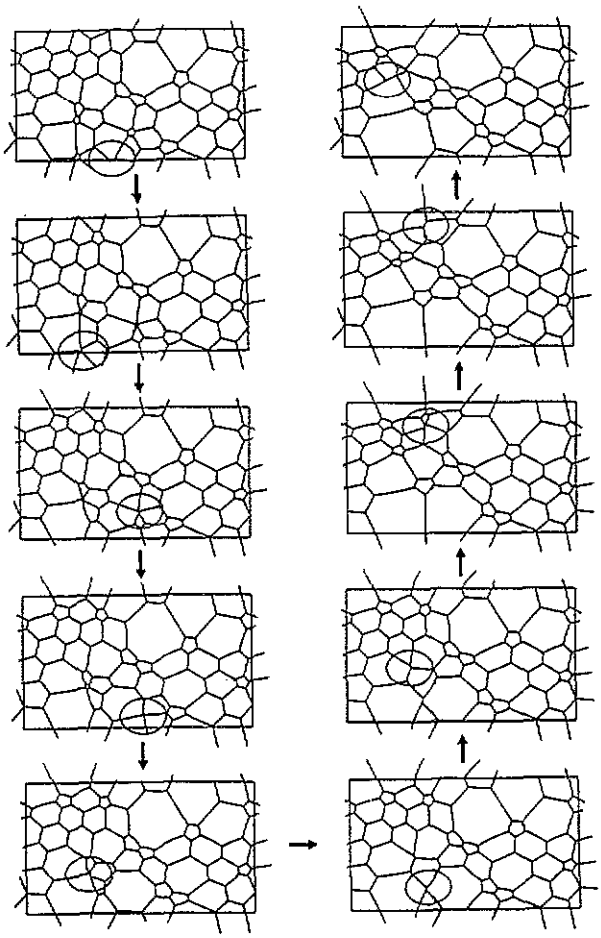

Figure 11. Avalanche of cell eliminations. Attention is drawn to the locations of local topological changes by the superimposed ellipses. The sequence takes the structure from that of figure 8(*b*) to that of figure 8(*c*), upon a small increment of λ at $\lambda = 0.49$.

Some examples of the cell side distribution function $f(n)$ are also shown in figure 10, which are in quite good agreement with experimental data (Babcock *et al* 1990). For further discussion of this distribution, see section 6.

The avalanches seem to have the same character as those observed by Babcock and Westervelt (1990). Figure 11 shows an avalanche that eliminates ten cells. It represents the transition from figure 8(*b*) to (*c*). It would be most interesting to extend such calculations to much larger samples, in order to accumulate better statistics. Experience with the soap froth program would suggest that samples of 10^3 cells could be handled easily, but limitations of resources have kept the calculations presented here at a modest level.

6. Topological analysis

Although present results for the coarsening behaviour of the model are inadequate to show any detailed correspondence to the evolution of magnetic froth, it is very reassuring that the distribution function $f(n)$ corresponds quite closely to that of experiment.

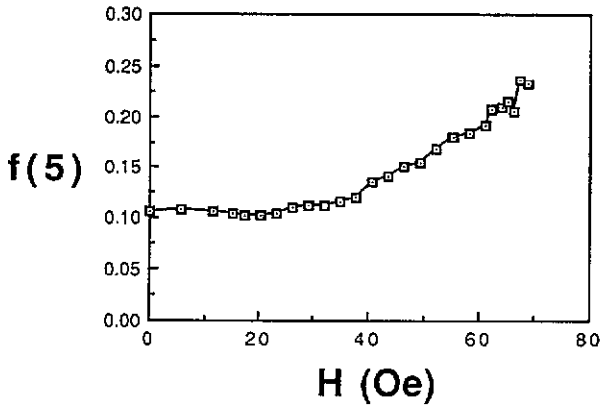

Figure 12. Observed variation of $f(5)$ with applied magnetic field H.

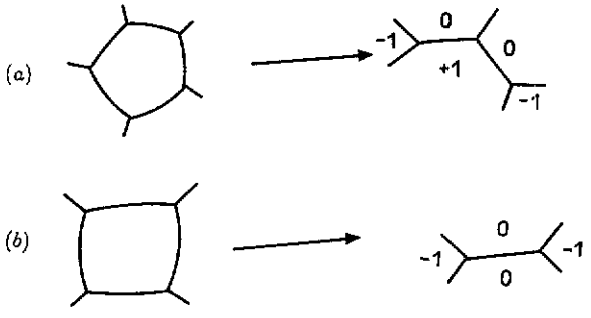

Figure 13. (*a*) Topological process: disappearance of a five-sided cell. The numbers indicate the change of number of sides of each neighbouring cell. (*b*) Disappearance of a four-sided cell (created by the process shown in (*a*)).

In this section we shall comment further on the form $f(n)$, using a purely topological analysis.

The observed invariance of $f(n)$ over two decades of cell density, reported by Babcock *et al* (1990), was not precisely reproduced in the experimental studies described here. However, it would appear that, in the relevant regime (roughly that described as 'intermediate' in section 2), $f(5)$ increases, as shown in figure 12, toward the value found to be invariant in the earlier work. (This value was stated to be 0.20 but the published data suggest that any value in the range 0.20–0.25 might be inferred.)

It would thus appear that, while much depends on the starting conditions, as one might expect, there is indeed a steady state, towards which the network tends in this regime. Let us therefore consider the effect of elimination of individual five-sided cells, as described above.

Topologically, such an event proceeds as shown in figure 13(*a*). The outcome shown is unique (apart from rotation or reversal of the external cell edges). We assume that a steady $f(n)$ is reached by the repeated occurrence of this process, after which it does not, on average, change $f(n)$. In order to express this, we must make assumptions regarding the neighbours of a disappearing five-sided cell, in relation to figure 13(*a*). We

make the most elementary assumptions: that the neighbours are (on average) distributed according to $f(n)$ itself, and that the individual values of n do not correlate with the outcomes shown in the figure. Both points require some justification.

Firstly, the assumption of the distribution $f(n)$ appears to contradict the Aboav–Weaire correlation, which implies that the neighbours of five-sided cells have a mean $\bar{n}$ *not* equal to 6, the mean of $f(n)$. However, the argument being advanced applies not to all five-sided cells but to five-sided cells on the point of disappearance, which will tend to be surrounded by cells somewhat smaller than the average. This argues for a correction in the opposite sense and, in the absence of a deeper analysis, the stated assumption seems best. In any case the suggested corrections are small.

Secondly, the assumption of random assignment of outcome seems a bold one, but Babcock and Westervelt (1989b) specifically assert that they could find no rule for such assignments in observing a sample of individual events.

We shall apply the steady-state condition firstly to the population of five-sided cells. Elimination of a five-sided cell by the process under consideration *directly* removes one such cell, and creates/removes others by virtue of the effect upon neighbours. In particular the subtraction of one side from a neighbouring five-sided cell creates a four-sided cell that is unstable, and must be eliminated by the process shown in figure 13(b). We shall make the same assumptions regarding this process as for that of figure 13(a), decoupling the statistics of the two events. Since we may now subtract one side from a further five-sided cell, there is a possible *cascade* of cell eliminations. On the above assumptions the total number of cells eliminated is

$$1 + 2f(5)(1 + 2f(5)\ldots) = 1/(1 - 2f(5)). \tag{10}$$

For steady state, the elimination of this number of cells must change the number of five-sided cells by

$$\Delta f(5) = -f(5)/(1 - 2f(5)). \tag{11}$$

Enumerating the various outcomes that contribute to $\Delta f(5)$ we have

$$-1 + 2f(6) - 3f(5) + 2f(5)(2f(6) - 2f(5))/(1 - 2f(5)) = -f(5)/(1 - 2f(5)) \tag{12}$$

or

$$f(6) = \frac{(1 - 2f(5)^2)}{2}. \tag{13}$$

Suppose we assume that $f(n) = 0$ for $n > 7$. Then, requiring $f(n)$ to be normalized to unity, and to have the (Euler) mean value 6,

$$f(5) + f(6) + f(7) = 1 \tag{14}$$

$$f(5) = f(7). \tag{15}$$

Hence

$$f(5) = \tfrac{1}{2}(1 - f(6)) \tag{16}$$

which may be used, in conjunction with (13), to determine $f(5)$. The result is $f(5) = 0.29$ $(= f(7))$, $f(6) = 0.42$ (and second moment $\mu_2 = 0.58$), in good agreement with the experimental values. However, it should be noted that this was obtained by using a rather arbitrary assumption, that $f(n)$ goes to zero so rapidly that we may neglect $f(n)$

for $n > 7$. One may instead write a similar equation for general n, and proceed to solve it, but some additional assumption would be needed to specify a solution. (The Euler and normalization conditions are automatically satisfied.)

7. Conclusions

The approximate model based on the soap froth and the statistical argument of the last section provide a promising framework for the understanding of cellular domains in magnetic froth.

Problems for further consideration include the simulation of the 'melting' of ordered domains and the associated phase diagram, as well as the detailed description of the regime close to the limiting magnetic field, at which the wall width goes to zero. This has multiple effects, not easily analysed: appropriate simulations may help. However, the latter will be hindered by the 'avalanche' character of coarsening in this regime, making the gathering of adequate numerical data difficult.

It should be emphasized that simulations within this model can be pursued within much larger samples than were presented here, probably in excess of 10^3 cells. Limitations of time and resources confined the present work to an exploratory study.

Acknowledgments

D Weaire wishes to thank the University of California at Davis for hospitality over the period during which much of this work was undertaken and EOLAS (Irish Science and Technology Agency) for research support. P Molho wishes to thank M Magnasco, who was involved in the processing of experimental data, and A Libchaber, who initiated the experiment at the University of Chicago.

Appendix A. Experimental details

The experimental data reproduced here were obtained using a monocrystalline film of the ferrimagnetic garnet $(YLuBi)_3(FeGa)_5O_{12}$ provided by LETI–CENG, Grenoble. The film thickness was 5.33 μm and the stripe width in zero field was 5.50 μm. Other material parameters were as follows: magnetization, 188 G; Curie temperature, 130 °C; characteristic length (wall energy density divided by magnetic energy density), 0.63 μm.

Pictures of domain patterns of size $(7–11) \times 10^4$ μm^2 were processed as 640×480 pixels. The experimental conditions were as follows. The pictures shown in figure 1 were obtained at room temperature with no AC field superimposed on the bias field. (For the significance of applied AC field see Babcock and Westervelt (1989b).) For the data of figures 3, 4 and 12, an AC field of amplitude 3 Oe was superimposed and the pixel size is 0.3625 μm^2/pixel.

Appendix B. Mathematical background

In this Appendix, we consider the dependence of the magnetic dipolar energy on the structure of the cellular domain network. In this network, regions of 'up' magnetization are contained in cells bonded by thin walls of 'down' magnetization. We treat these walls

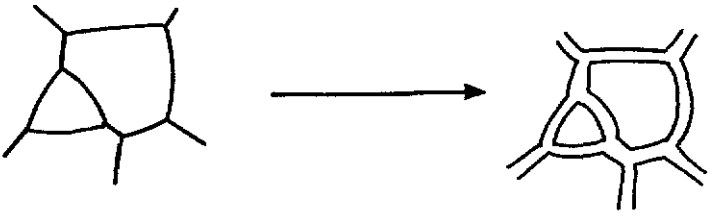

Figure 14. Dissection of cell network into separated cells.

as lines, in which case it is easy to show that the dipolar interaction energy may be written as

$$I = \frac{1}{2}\int \frac{dl\, dl'}{r_{ll'}^3}$$

where the double integral is over the cell wall network. However, this integral diverges, and it is necessary to introduce a short-range cut-off at $r = \Delta r$ to suppress this divergence. With such a cut-off, the integral I for a single cell, approximated by a circle of radius r, may be determined analytically; for small Δr it is given by

$$I \simeq -\frac{\pi}{16r} - \frac{\pi}{8r}\log\frac{\Delta r}{4r} + \frac{\pi r}{2\Delta r^2}.$$

For small Δr this may be further approximated the sum of two positive terms proportional to r and r^{-1} respectively. We have made the further assumption of identifying these two terms with the line length and inverse square root of area respectively, hence generalizing to the case of a non-circular cell. The cell–cell interaction of the second-order model is based on a more justifiable, if crude, approximation suggested by figure 14—namely, lumping the two cells in question into point dipoles with moments and separations estimated in terms of their areas. The latter is straightforward for nearest neighbours, leading to (8).

Although the present model is capable of only a limited justification by such arguments, a more systematic analysis should be possible. In particular, the functions of cell area could include the number of cell sides as further variables, without detracting from the practicality of the model.

References

Babcock K L, Seshadri R and Westervelt R M 1990 *Phys. Rev.* **41** 1952–62
Babcock K L and Westervelt R M 1989a *Phys. Rev. Lett.* **63** 175–8
—— 1989b *Phys. Rev.* **40** 2022–37
—— 1990 *Phys. Rev. Lett.* **64** 2168–71
Glazier J A 1989 *PhD Dissertation* University of Chicago
Glazier J A, Anderson M P and Grest G S 1990 *Phil. Mag.* B **62** 615
Glazier J A, Gross P S and Stavans J 1987 *Phys. Rev.* A **36** 306
Kermode P and Weaire D 1990 *Comput. Phys. Commun.* **60** 75
Weaire D 1989 *Phys. World* December, p 23
Weaire D and Bolton F 1990 *Phys. Rev. Lett.* **65** 3449
Weaire D and Lei H 1990 *Phil. Mag. Lett.* **62** 47
Wolfe R and North J C 1974 *Appl. Phys. Lett.* **25** 122–4